Impact of sample saturation on the detected porosity of hardened concrete using low temperature calorimetry

Min Wu*, Björn Johannesson

Department of Civil Engineering, Building 118, Technical University of Denmark, 2800 Lyngby, Denmark

Abstract

The present work studied the impact of sample saturation on the analysis of pore volume and pore size distribution by low temperature (micro-)calorimetry. The theoretical background was examined, which emphasizes that the freezing/melting temperature of water/ice confined in non-fully saturated pores is further depressed compared with that when the pores are fully saturated. The study of the experimental data on hardened concrete samples showed that for a same concrete mix, the total pore volume detected from the capillary saturated samples was always lower than that of the vacuum saturated samples and a higher proportion of pores with small radii were found in the capillary saturated samples. In addition, the observed hysteresis between the freezing and melting curves of ice content of the capillary saturated samples was more pronounced than that of the vacuum saturated samples. The major reason for the observed phenomena could be related to that capillary saturation cannot fully saturate the pores under study.

Keywords: Concrete, calorimetry, freezing and thawing, pore size distribution, hysteresis, thermoporometry.

1. Introduction

Porosity is one of the most important characteristics of cement based materials. It is the main parameter which determines strength and influences transport properties or permeability. For this reason, it is also a major parameter determining durability. Thus considerable efforts have been devoted to the characterization of the pore structures for cement based materials.

The pore system in a cement based material is rather complicated, e.g., in terms of the pore size. There are different types of pores existing in one single cement based material. There are deliberately entrained air voids with diameters on the order of 50–100 μm for frost protection [1, 2]. Mixing and casting of concrete, however, could entrap air voids whose size can reach the millimeter scale [3]. Meanwhile, there are nano-microscale "capillary pores" that are remnants of the interstitial spaces between the unhydrated cement grains [4]. Additionally, as described, e.g., in [5, 6], there are interlayer spaces, or "gel pores" at the nanometric level between the primary particles of the hydration products calcium-silicate-hydrate (C-S-H). It is further argued by Sun and Scherer [7]: since the pore space in a cement based material can be fully interconnected, as indicated by the fact that the liquid can be fully exchanged by solvents, the definition of a pore size or shape is thus quite arbitrary, because there is actually only one interconnected pore with a very complicated shape.

Many methods for porosity characterization have been developed and applied to cement based materials [7–12], e.g., nitrogen adsorption/desorption (NAD), mercury intrusion porosimetry (MIP), scanning electron microscopy (SEM), scattering of X-rays or neutrons, low temperature calorimetry (LTC), nuclear magnetic resonance (NMR), moisture fixation, etc. A summarized comparison about these different methods can be found, e.g., in [7]. The measurement of NAD gives good information for mesopores (IUPAC classification) while it is not suitable to characterize capillary pores. MIP measures the pore entry radii rather than the interior pore sizes, since mercury can be intruded into some large pores through the small entrances (e.g., ink-bottle shaped pores). Optical microscopy and SEM are able to reveal the size of large pores but they are not able to resolve the mesopores. Moreover, a major disadvantage shared by NAD, MIP and SEM (including environmental SEM) is that the testing samples must be dried. For cement based materials this drying process often results in an apparent alteration of pore structure under consideration [13].

Calorimetric methods have been used to study cement based materials for a long time, e.g., see [14–18]. Low temperature (micro-)calorimetry or LTC, which is also known as thermoporosimetry and sometimes is referred to as thermoporometry or cryoporometry as well, can be applied to characterize the porosity of virgin cement based samples without any drying treatment [10, 19–22]. The basic concept of LTC is that the freezing process of water is an exothermic process and the melting process of ice is an endothermic one, from which the ice content can be calculated by using the heat of fusion for the confined water/ice in the freezing or the melting process and the measured heat flow with respect to ice formation or melting at different measuring temperatures. If a sample is fully saturated with water, then the volume of the ice formed/melted under different temperatures in a sense indicates the pore information of the sample under the testing. By making certain assumptions, thermodynamics demonstrate there is a unique equation showing the correspondence between the phase transition temperature of the water confined in pores and the curvature of its solid-liquid interface under the condition that the sample is fully saturated [23, 24]. By studying the thermodynamic parameters of the confined water/ice, the quantitative relation of the freezing/melting temperature and the pore size can be determined.

Although LTC is often adopted as a method to study the porosity of a porous material, the analysis of the experimental data is not that straightforward. The factors which influence the accurate interpretation of the results include: the mechanism of ice formation in pores, baseline calculation, heat of fusion for water/ice confined in small pores, supercooling effect, the ions in the pore solution, the thickness of a water layer very close to the pore walls, temperature lag between the thermopile of the instrument and a testing sample, etc. It has been discussed, e.g., in [7, 24–27] that there is a hysteresis behavior between the freezing and the melting process in terms of the determined ice content curves. Thus, the mechanism of ice formation in pores turns out to be very important since it would decide which process is more appropriate to be adopted to calculate the pore sizes. The mechanism of ice formation in small pores has been studied rather extensively and there are two representative assumptions in this regard, i.e., homogenous nucleation and progressive penetration following heterogeneous nucleation, e.g., in [7, 24, 28–30]. Homogenous nucleation indicates that the ice nuclei appear spontaneously in the liquid water and that the ice will be formed when the critical size of the nuclei (at a given temperature) is the same as that of the pore [24, 28]. Brun et al. assumed in a series of work, e.g., in [24, 31, 32], that the ice formation process is a homogenous nucleation process. If this assumption is correct, the pore sizes detected in the freezing process is the interior (or real) sizes of the pores and then it is possible to use the freezing process to analyze the interior pore size distribution. However, studies by many authors show that the probability of homogenous nucleation governing the whole ice formation process is

low and only when the temperatures is on the order of −38 °C will the homogenous nucleation become significant [29, 33, 34]. Thus, it is normally accepted that the freezing of water in pores should be initiated by heterogeneous nucleation and then followed by a progressive penetration of the ice front from big pores to small pores, e.g., in [7, 10, 15, 29, 35, 36]. In that case, it is only possible to derive some information about the pore entry sizes, rather than the interior pore sizes, from the freezing process (some more discussions about the freezing process will be presented later combined with the measured experimental data). Then the melting process, which is assumed to reflect the interior pore sizes, is suggested to be used to calculate the pore size distribution. Based on the above discussion, probably both the freezing and the melting process should be analyzed as the freezing process may provide information about the pore entries while the melting process may reflect the interior pore size information.

There are some other topics that need to be considered in analyzing heat flow curves. The baseline calculation and the heat of fusion of pore confined water/ice are two fundamental aspects in analyzing the ice content from experimental data. The discussions about the baseline calculation can be found, e.g., in [7, 17, 37, 38]. Many efforts have been devoted to obtaining the heat of fusion of water/ice confined in small pores, e.g., see [24, 26, 37, 39, 40]. A summarized discussion about the influence of these two aspects can be found in [41]. Supercooling refers to the phenomenon that bulk water does not freeze at 0°C, which is often attributed to the lack of nucleation sites. If the supercooling is very pronounced, it is not possible to derive the pore entry size information corresponding to the temperatures which are higher than the freezing point of the supecooled water based on the freezing curve. In order to address this issue, two freezing and melting cycles are often adopted. Followed by the first freezing process, the sample will be heated to a temperature just below the melting point of the water in macropores. During the second freezing process, the ice crystals left in the macropores or on the exterior surface of the sample after the first melting process will serve as the nucleation sites. By doing the two cycles experiment, supercooling is expected to be avoided and then both the entry and interior sizes of the mesopores can be determined based on the measured data of the second freezing and melting process respectively. More related discussion can be found, e.g., in [7, 35, 36, 42].

It is normally assumed that there is a portion of water which is very close to the pore walls and it will not undergo phase transition even if the temperature is very low. Banys et al. [43] estimated that the water in this layer would only freeze at a temperature between 21 and 26 K. This layer, which will be referred to as $\delta-$layer, will definitely affect the derivation of the total pore volume and the pore size distribution. Fagerlund [15] correlated the $\delta-$layer with the adsorbed layer in moisture fixation experiments and arrived at an equation showing the thickness of the $\delta-$layer can be expressed as a temperature dependent function. Normally the $\delta-$layer is treated as consisting of 2-3 layers of water molecules, which corresponds to about 0.8 nm in thickness, e.g., in [24, 42, 44]. Sun and Scherer [7] suggested that in mortar samples, it is more reasonable to use a value of 1.0-1.2 nm for this $\delta-$layer due to the dissolved ions in the pore water.

The present study focuses on the impact of the sample saturation on the analysis of pore volume and pore size distribution by the LTC method. For LTC measurements, the samples to be tested need to be fully saturated with water before putting into a calorimeter. If a sample is not fully saturated, firstly the pores which are not filled with water will not be detected and as a result, the total volume of the pores will be underestimated. Furthermore, the correlation between the pore size and the depressed freezing/melting temperature in the context of pore size determination is normally based on the prerequisite that the pores under study are fully saturated, e.g., see [24, 26]. However, a careful examination of the theoretical background in this study emphasizes that the

thermodynamic correlation for fully saturated pores is different from that for non-fully saturated pores. Moreover, the correlation for the non-fully saturated system could be very complicated, which is extremely difficult to characterize quantitatively, if it is still possible. Under such cases, the calculated pore sizes will not be correct any more if the pores are not fully saturated while we still use the relation as derived based on the full saturation assumption. Based on the experimental data measured on hardened concrete samples conditioned by capillary saturation (samples submerged in water) and vacuum saturation, the ice content, pore volume and pore size distribution are calculated to demonstrate the impact of sample saturation on the porosity analysis.

2. Theoretical background

To illustrate the impact of sample saturation on the determined pore size distribution, the relation between the depressed freezing point of a liquid confined in a pore and the pore size should be introduced. The detailed derivation of the relation based on thermodynamics and related discussions can be found, e.g., in [23, 24, 29, 36]. It should be mentioned that even though the thermodynamic approach is widely used, the applicability of this approach to nanoscopic systems has been questioned by, e.g., Setzer in [45, 46], since the thermodynamics used are completely macroscopic. That is, the smallest pore size detected using the thermodynamic approach may be limited. However, with no more knowledge, the traditional way of using thermodynamics is followed in this work.

As pointed out by Brun et al. [24], in order to calculate the freezing/melting point of a liquid/solid confined in a pore system where the three phases (liquid, solid, gas) of the confined substance coexist, it is necessary to know two curvatures of the three interfaces (liquid-solid, liquid-gas and solid-gas). However, this condition can not usually be met for a porous material under study. The situation will become much simpler if the porous material is fully saturated with water, which means the solid/gas interface is plane (i.e., the curvature is always zero during freezing and melting). Under such circumstances, the depressed freezing or melting temperature is only determined by the curvature of the solid/liquid interface which can be directly related to the size of the pores where the water or ice is confined. The relation can be expressed as

$$\Delta S_f dT = v_l d(\gamma_{sl} \frac{dA_{sl}}{dV_l}) \tag{1}$$

where $\Delta S_f = s_l - s_s$ is the specific entropy difference between the liquid and the solid phase ; T is the temperature (in Kelvin degree); v_l is the specific volume of the liquid phase; γ_{sl} is the surface tension and dA_{sl}/dV_l is the curvature of the liquid-solid interface. It is noted that Eq.1 is usually adopted to do the pore size analysis in the context of LTC. From the discussion, it is clear that there is a prerequisite to use Eq.1, which is that the pores of the material under study must be fully saturated. If this condition is not met, the relation between the depressed freezing/melting point of the confined water/ice and the pore size as derived based on Eq.1 does not hold. Still abiding by Eq.1 to calculate the pore size distribution for a non-fully saturated pore system, the result could be in doubt.

For non-fully saturated pore systems, the possible situations for what can happen to the menisci system when water/ice freezes/melts were discussed, e.g., in [23, 24]. Fridh [38] reviewed and summarized the discussion in this aspect. As shown in Figure 1, the three possibilities of the coexisting phases include: (1) both the solid phase (s=solid) and the pore liquid (l=liquid) are exposed to the gas (g=gas) but not to each other (Case A); (2) the pore liquid is in contact with

both the solid and the gas (Case B); (3) the solid phase is in contact with both the gas and the pore liquid (Case C).

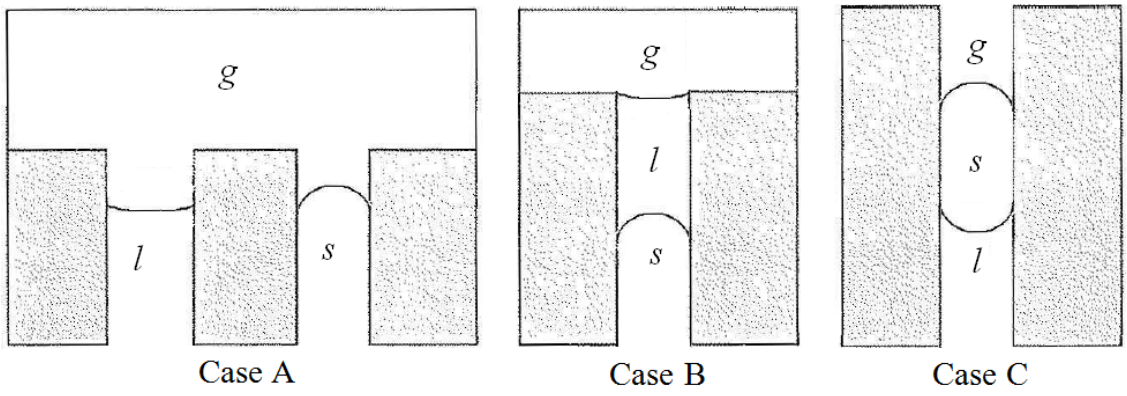

Figure 1: Schematic illustration of the possible menisci systems found in a porous material during freezing, water being the substance confined in the pores. The illustration is based on the figure presented in [38] but with reversed curvature of solid-gas and solid-liquid interfaces.

For Case A, the relation between the depressed freezing point and the curvature of the interfaces can be expressed as Eq.2; for Case B and Case C, Eq.3 and Eq.4 are valid, where r_{lg} , r_{sg} and r_{ls} are the radii of the interfaces which are not necessarily equal to each other and $\triangle H_{fus}$ is the heat of fusion for the confined water; v_i is the specific volume of the phases (l, s, g); T is the freezing/melting point of the confined liquid/solid and T_o is that of the bulk liquid/solid. It should be noted that the equations (Eq.2, Eq.3 and Eq.4) presented here are slightly different from that presented in [38] and a reversal of the curvatures of the solid-gas and the solid-liquid remedies the differences.

By studying Eq.2 to Eq.4 carefully, it can be found the relation between the depressed freezing point of the water and the curvature of the interfaces becomes much more complicated if some of the three phases coexist simultaneously. Thus, it is very difficult, if it is still possible, to quantify the relation between the pore size and the depressed freezing/melting temperature of the confined water/ice since as one lacks the knowledge about under which case(s) the pores are and how many pores there are under each case (referring to the three cases in Figure 1). However, if a porous material is, or at least the pores under study are, fully saturated with water, the case becomes much simpler and clearer. By substituting the gas phase (g) with liquid phase (l) in Figure 1, there will be only one interface, i.e., the liquid-solid interface. Then accordingly, the relation between the radius of the curvature and the depressed freezing point can be explicitly represented by Eq.4 without considering the second term in the parenthesis on the right hand, or its equivalent form Eq.1 (differential form, $\triangle H_{fus} = T \triangle S_f$), e.g., see [24, 47, 48].

$$\ln \frac{T}{T_0} = -\frac{2}{\triangle H_{fus}} \left(\frac{v_l \gamma_{lg}}{r_{lg}} + \frac{v_s \gamma_{sg}}{r_{sg}} \right) \tag{2}$$

$$\ln \frac{T}{T_0} = -\frac{2}{\triangle H_{fus}} \left(\frac{v_s \gamma_{ls}}{r_{ls}} + \frac{v_s - v_l}{r_{lg}} \cdot \gamma_{lg} \right) \tag{3}$$

$$\ln\frac{T}{T_0} = -\frac{2}{\triangle H_{fus}}\left(\frac{v_l\gamma_{ls}}{r_{ls}} + \frac{v_s - v_l}{r_{sg}} \cdot \gamma_{sg}\right) \tag{4}$$

With respect to water, we have $\gamma_{lg} > \gamma_{ls}$ and $v_s > v_l$ [38, 47]. Then, by comparing Eq.2 to Eq.4 with Eq.1, we conclude that the freezing/melting temperature of the confined water will be further depressed if the pores under study are only partially saturated compared with the fully saturated counterparts, no matter the non-fully saturated pores are under which case (i.e., the three cases in Figure 1). The effect of the curvature of the liquid-gas interface (see Eq.3) and that of the solid-gas interface (see Eq.4) in a non-fully saturated system on the depressed freezing/melting temperatures was also discussed by Blachere and Young [49] and Williams [48] respectively. Related discussions in this aspect can also be found in, e.g., in [15, 23, 24]. A more recent study [50] measured the melting behavior of a model pore system conditioned with different saturation degree before the freezing and it was demonstrated that the melting curves are shifted to some lower temperatures as the saturation degree lowers, in which the low saturation degree means some of the pores are not fully saturated. This can be a very direct experimental validation supporting the argument discussed above, i.e., the further depressed freezing/melting point of the water in non-fully saturated pore systems.

It should be mentioned that due to the fact that water in very small pores does not freeze and the freezing/melting point depression of water/ice in big pores is too small, the pores that can be studied by LTC are limited mainly to mesopores with the reliable pore radii between about 2 nm to about 40 or 50 nm [7, 36]. Then one may argue that to determine pore size distribution (PSD), e.g., for cement based materials, it does not matter whether the big air voids are fully saturated or not, since the concerned pores are small mesopores. As far as the small mesopores can be fully saturated by capillary saturation, which is possible considering the capillary force [51], the PSD determination should not be affected by the saturation status of the big air voids. Using the same calculation method, the calculated PSD curves for samples conditioned by capillary and vacuum saturation will be compared to illustrate the impact of sample saturation on the PSD determination.

3. Experimental data

The present investigation is based on existing experimental data. The details of the experimental study and the data can be found in [17, 52, 53].

The concrete samples with three different water-to-cement ratios, each with different nominal 'target' air contents were prepared. The cement content for the w/c=0.4 concrete samples with nominal air contents of 2%, 4% and 6% were 515, 525 and 525 kg/m^3 respectively. And the corresponding values for the w/c=0.5 and w/c=0.6 samples were 475, 480 and 480 kg/m^3 and 340, 350 and 335 kg/m^3. Granite aggregate with two different size ranges, i.e., 0-3 mm and 4-8 mm, and approximately equal amount of the two fractions of the aggregate were used to prepare all the mixes. Air-entraining agent was used to produce the concrete with nominal air content 4% and 6%. The concrete samples were produced in 120L batches in the laboratory. The fresh concrete was placed into two moulds with the dimension of 200mm×500mm×500mm and into cubic moulds with the dimension of 100mm×100mm×100mm after mixing. The moulds filled with fresh concrete were vibrated for a few seconds, and then a plastic film was used to prevent evaporation. After curing under sealed condition for one day, the concrete was core-drilled and sawn into small cylinders with the diameter of 14mm and the length of 60mm. The size of the samples was chosen to fit the calorimetric device adopted in the investigation. The cylindrical samples were stored in a small

bucket with about 1 liter water to cure the samples at about 20°C. And they were divided into two groups in measurement: one group of the samples were stored till about four months before testing (capillary saturation) and the other group were also water cured till about the same age but were vacuum saturated before testing (vacuum saturation).

Figure 2: Top of the SETARAM scanning calorimeter showing the liquid nitrogen supply tube and the reference and sample chamber [17].

A Calvet-type scanning calorimeter (SETARAM) was used for this investigation, as shown in Figure 2, which was calibrated and operated to work between about 20 °C and -130 °C. The temperature scanning consisted of a cycle starting at 20 °C and going down to about -80 °C and then back to 20 °C. The adopted cooling and heating rate was 0.09 °C per minute. The samples were saturated surface dry when placed in the calorimeter. A dried (under about 105 °C till constant weight) concrete sample, of the same dimension as the testing specimen, was used as the reference sample. In the investigation, the same reference was used throughout all the tests. By using this type of reference sample, it simplifies the calibration of the measurement compared to the use of other materials such as aluminum. There are some discussions about the necessity of using a reference sample in the calorimetric experiments. Actually, the heat capacity of the solid skeleton of a porous material may vary to a certain degree under different temperatures and this variation can be further reduced if a reference sample, which is of the same size as the material used in the sample chamber but dried, is used in the experiment. More discussion in this regard can be found in [41]. During the testing, the calorimeter records the calibrated heat supplied to or released from the specimen. This means that the instrument measures the difference of the heat flow between the reference and the sample vessel, thus the heat flow due to the confined water and its phase transition in a sample at different temperatures can be determined. At the same time, the corresponding actual temperature in the sample chamber is also recorded. By using the measurement heat flow and the thermodynamic parameters for the confined water, it is possible to determine the ice content, which is an indication of the ice filled pore volume, under different temperatures.

After a calorimetric measurement, the sample was dried under about 105 °C till constant weight. By doing so, the total water content of the sample was determined by the mass difference between this dried state and that before the calorimetric measurement (saturated surface dry). The total porosity of the concrete mixes studied were also determined through gravimetric measurements by measuring the mass of the sample both in air and submerged in water using the vacuum saturated samples.

4. Results and discussion

4.1. Volume of ice in hardened concrete samples

An accurate analysis of the measured LTC data is the basis to calculate the pore volume and pore size distribution for a porous material. Two fundamental aspects are crucial in this context, i.e., the baseline calculation of the measured heat flow and the value of the heat of fusion for the water confined in pores. The detailed discussion and the calculation scheme for determining the ice content can be found in [41].

The calculated results of the total ice volume by the total volume of the concrete sample are shown in Figure 3. It can been found that for each concrete mix, the ice volume determined for the capillary saturated samples both in the freezing and the melting process are always smaller than that for the vacuum saturated samples. It implies that there is a portion of pores which are not filled by water in the capillary saturated samples. Since the LTC method can only detect the pores which are filled with water, these unfilled pores will not be detected. For the concrete mixes with the same w/c under study, the difference of the total ice volume fraction between the capillary saturated sample and the vacuum saturated sample increases as the nominal air content increases. Compared with the vacuum saturated samples, the hysteresis effect, as demonstrated by the distance between the freezing curve and the melting curve at the same temperature, is more pronounced for the capillary saturated samples under most of the temperatures in testing, e.g., from -10 °C to -40 °C. This phenomenon was also pointed out in [17].

The fraction of the maximum ice volume by the total volume of the sample for the concrete mixes presented in Figure 3 are listed in Table 1. For the calculation method adopted, there is small difference between the ice volume fraction calculated from the freezing and melting process in one cycle for each concrete sample. The result for a sample listed in Table 1 is the average value of the freezing and the melting process. With respect to the concrete mixes with w/c=0.4, the maximum ice volume fraction calculated for the vacuum saturated sample and the capillary saturated sample differ by 2.1% for sample C404; while the difference becomes 3.1% for sample C406. This difference for sample C504 and C506 are 1.2% and 3.4% respectively. The trend that the difference of the maximum ice volume fraction increases as the air content increases, can also be found for the samples with w/c=0.6. The difference for sample C602 is 1.2% and it increases up to 6.3% for sample C606. A possible indication of this phenomenon is that it may be difficult to saturate all of pores, especially the entrained air voids whose diameters are often on the order of 50-100 μm [1, 7], with water by the capillary saturation method. However, with the vacuum saturation method, the case could be different. Taking sample C606 as an example, the entrained air content is about 5.2% (by comparing the measured air content of sample C602 with no air-entraining agent and that of C606 with air-entraining agent); while the calculated difference of the ice volume fraction between the vacuum and capillary saturated samples is 5.0%. The difference of the ice volume is very close to the volume of the entrained air. By studying the difference of the ice volume fraction in the samples of the same w/c treated with vacuum saturation method, it is

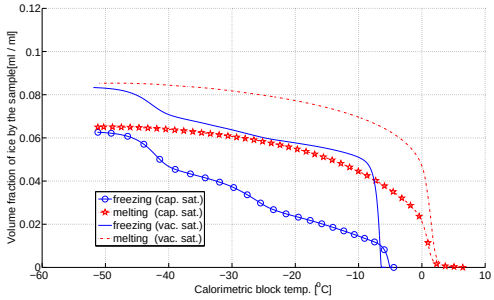

(a) w/c=0.4, nom. air cont 4%.

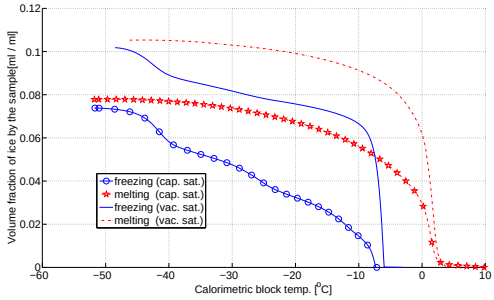

(b) w/c=0.4, nom. air cont 6%.

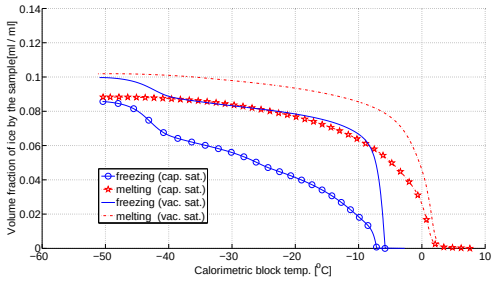

(c) w/c=0.5, nom. air cont 4%.

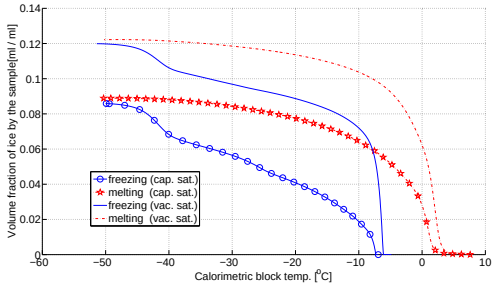

(d) w/c=0.5, nom. air cont 6%.

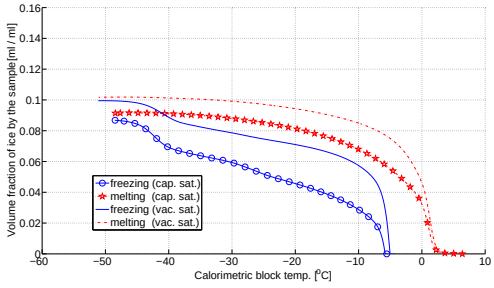

(e) w/c=0.6, nom. air cont 2%.

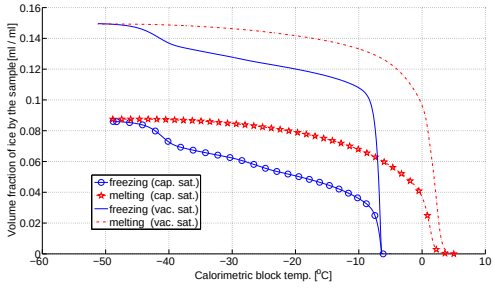

(f) w/c=0.6, nom. air cont 6%.

Figure 3: Calculated fraction of the ice volume by the total volume of the sample for capillary saturated (cap. sat.) and vacuum saturated (vac. sat.) concrete samples. The nominal air content is denoted for each mix and the corresponding measured air content is shown in Table 1.

found that the difference is very close to or a little bit higher than the difference of the measured air contents. That is to say possibly after vacuum saturation all of the air voids are filled with water in the concrete samples. If the big pores, i.e., those whose pore sizes are on the same order of the entrained air voids, are filled with water, the possibility for the smaller ones (i.e those in the nm scale) to be saturated with water is high due to the capillary suction pressure [51].

It is also noticed that RILEM [54] recommended a test method by applying vacuum to reach full saturation for concrete samples, though the applicability of this method on high strength concrete is argued and pressure saturation is proposed by some authors, e.g., see [55–57]. Since the concrete in our study is not high strength concrete and based on the above discussion of the experimental data, we tend to think that the concrete samples are almost fully saturated by vacuum saturation method. On the other hand, one main purpose of this study is to demonstrate how the thermodynamic relation can be affected by the non-fully saturated pores and hence the impact on the determination of the pore size distribution. Even if the vacuum saturation cannot absolutely fully saturate the pores in concrete samples, it would be reasonable to expect that only a small volume of pores is left unsaturated. Then the impact of the small volume of unsaturated pores is considered negligible. In this sense, the concrete samples conditioned by vacuum saturation method is mentioned as fully saturated samples anyway in this study.

Table 1: The fraction of the maximum ice volume by the total volume of the sample for concrete samples presented in Figure 3. The notation for the sample C404 means that w/c=0.40, nominal air content 4%, and likewise for the other samples. The measured experimental data, including the approximate saturation degree of the capillary saturated samples, the measured air content and the porosity using vacuum saturated samples, are listed for the reference.

Sample	Fraction of maximum ice vol. (%)		Approx. saturation degree (cap. sat. samples)^{a,b}	Measured air content (%)^{a,c}	Porosity using vac. sat. samples (%)^{a,b,d}
	vac. sat.	cap. sat.			
C404	8.5	6.4	0.93	4.2	16.8
C406	10.7	7.6	0.81	6.1	18.1
C504	9.9	8.7	0.91	3.6	18.6
C506	12.1	8.7	0.78	5.4	21.6
C602	10.0	8.8	0.88	2.6	18.1
C606	15.0	8.7	0.68	7.8	23.2

Note: a). measured experimental data were given in [17]; b). it was assumed that the samples were fully saturated by vacuum saturation method; c). measured air content for the fresh concrete mixes (the measured air content for the samples C402 and C502, for which the LTC data are not analyzed here, are 2.6% and 2.0% respectively); d). gravimetric measurement.

4.2. Pore volume and pore size distribution

As can be found from the results shown in Figure 3, the supercooling effect is very obvious on the freezing curves. Consequently, it is not possible to derive the pore entry sizes whose corresponding freezing temperatures are higher than the supercooled temperature. Additionally, there is a relatively large increase of ice content in the freezing curve around the temperature of about -40°C for all the studied samples. This portion of ice is believed related to homogenous nucleation,

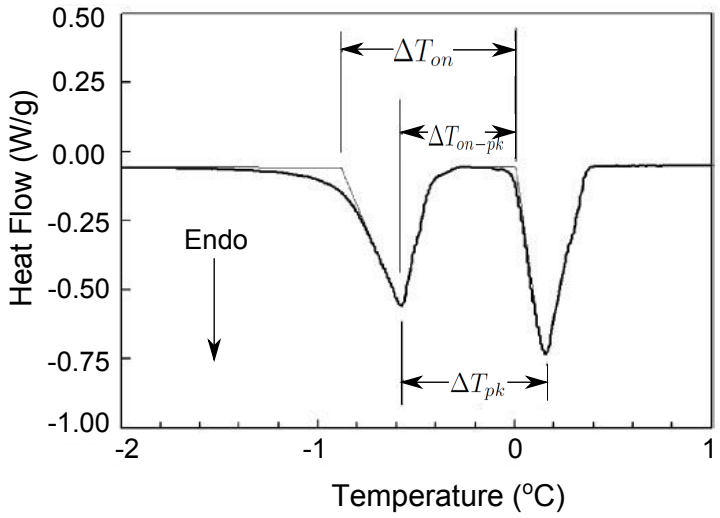

Figure 4: Three different methods to determined the temperature depression ΔT on the LTC melting curve: the peak-difference (ΔT_{pk}), onset-difference (ΔT_{on})and onset-peak difference (ΔT_{on-pk}) [36]. "Endo" denotes that the melting process is endothermic.

which does not necessarily reflect the pore entry sizes, e.g., see [29, 30, 47]. Due to this complexity, the pore entry size information will not be analyzed in this study and we will only adopt the melting curve to do the interior pore size distribution analysis.

It can be seen in Figure 3 that there is a portion of ice which melts above 0 °C in each concrete sample and the amount of this portion of ice is bigger in the vacuum saturated sample than that in the capillary saturated sample for the same concrete mix. This portion of the ice, most of which we believe are present in the relatively big air entrained pores in the concrete samples under our study (the surface dry samples were used in testing indicating very small amount of bulk water, if there is any), behaves like the bulk ice in terms of its heat flow characteristics. The heat flow behavior of bulk ice has been discussed, e.g., in studying the molecular sieve materials [36, 42, 44, 58–60]. It is due to the non-equilibrium between the testing sample and the instrument even if a very small sample (on the order of milligram) is used [36]. That is, the temperature as measured by the instrument is not the same as that in the sample. Consequently, the depressed freezing/melting temperatures should be calibrated accordingly. A detailed explanation about how to calibrate the temperature depression ΔT ($\triangle T = T - T_0$) and the influence of the different determination methods, e.g., in melting process, were conducted in [36]. As shown in Figure 4, the peak at the lower temperatures on the left side is due to the pore confinement effect and the other peak on the right side, which starts around 0°C, is due to the surplus bulk water added to the sample. The temperature corresponding to the peak of bulk water will be influenced by the adopted scanning rate and the amount of bulk water in the experiment. Three different methods to determine a better estimate of the ΔT, i.e., the the peak-difference (ΔT_{pk}), the extrapolated onset-difference (ΔT_{on}) and the extrapolated onset-peak difference (ΔT_{on-pk}), were compared for porous materials with a narrow pore size distribution. It was concluded that the onset-peak difference (ΔT_{on-pk}) is most appropriate to determine the ΔT, which shows small sensitivity to the adopted scanning rate and the amount of the surplus bulk water [36].

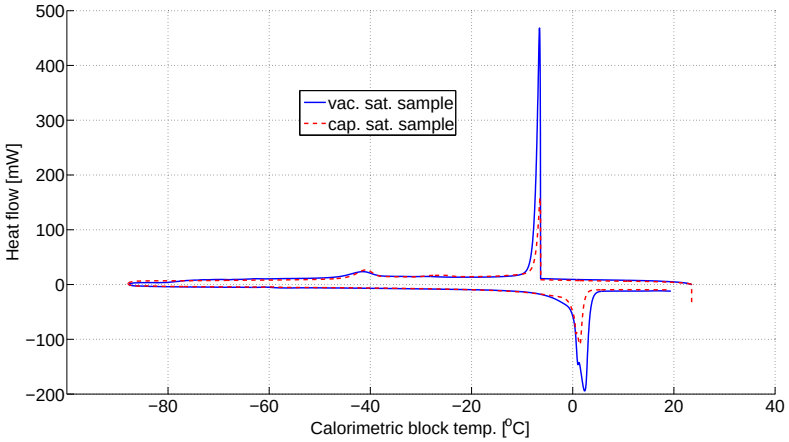

Figure 5: Measured output data from the LTC instrument, the heat flow versus the calorimetric block temperature, for concrete mix C606. The heat flow was recorded positive for the freezing process and negative for the melting process, respectively.

A typical measured output data from the LTC instrument are plotted in Figure 5. Unlike the porous materials with narrow pore size distribution, there is only one peak for the tested concrete samples on the melting curves, compared with the two peaks shown in Figure 4. That is probably mainly due to that the pore sizes of the concrete samples are widely distributed and the ice confined in the pores melts continuously, as a result showing no obvious separated peaks on the melting curves. Using the same method as adopted in [36], it is possible to extrapolate an onset melting temperature on the measured melting curve for a concrete sample. But, still it is not that straightforward to determine the depressed melting temperature ΔT corresponding to each measured temperature T. Because, as we know, the onset of the melting point as determined for the concrete samples in this study should be for the ice in entrained big air voids (on the order of μm) rather than that for the bulk ice. However, the depressed melting temperatures for the ice in the μm pores are already very small, e.g., $\Delta T \approx -0.03$ K for pore radius of 1μm and $\Delta T \approx -0.003$ K for pore radius of 10μm (based on Eq.5), compared with $\Delta T \approx 0$ K for bulk ice. It makes little sense trying to distinguish the pore sizes at this small level of melting point depression. As we have no clue to which pore radius the onset melting point should correspond, it is necessary to make an assumption. Here, an assumption is made that the extrapolated onset melting point, T_{on}, is corresponding to the melting point of ice confined in the pores with the pore radius of 1μm (since the sizes of the entrained air voids are on the order of μm), i.e., $T_{on} - T_0 = -0.03$ K. Then, the depressed melting temperature ΔT is calibrated based on the extrapolated onset melting point T_{on} and the measured melting temperature T. Actually, we can also assume the extrapolated onset melting temperature corresponds to the melting point of ice confined in the pores with radius of 500 nm, 10 μm or even to that of bulk ice. The calibrated melting point depression ΔT will not differ too much based on the different assumptions. Thus, the derived pore radii based on the calibrated ΔT (according to Eq.6 or Eq.5) in the range between 2 nm and 40 or 50 nm, i.e., the reliable pore radii for this LTC method as described before, will not be sensitive to the different assumptions made.

The ions in the pore solution and the thermal lag between the instrument and the concrete sample under testing affect the freezing/melting point of the confined water/ice. It should be noted that the measurement conditions will be kept the same for all the measurements and the ions concentration in the pore solution would not differ too much for all the mixes since the same cement is used. Thus, the effects due to the ions and the thermal lag should be more or less the same for all the concrete mixes under consideration in this investigation. Meanwhile, it is also noted that the effect due to the thermal lag and that due to the ions would cancel each other out to a certain degree. As the purpose of this study is to compare the difference caused by the sample saturation on the calculated porosity, both of these factors are considered. In order to derive the pore volume and the pore size distribution, we need to assume the thickness of the $\delta-$layer, δ. As mentioned before, there are different opinions with respect to the specific choice of the value of the δ. As the focus of this study is for comparison purpose, the δ is assumed to be 0.8 nm, as proposed by Brun et al. [24], for all the concrete samples considered. With respect to the relation between pore size and the depressed melting temperature, the numerical equations proposed by Brun et al. [24] based on Eq.1 is used. That is, Eq.5 is adopted for cylindrical pore assumption and Eq.6 for spherical assumption. Based on the calculated ice volume shown in Figure 3, the pore volume can be derived by Eq.7, where r is the radius of the ice crystal corresponding to certain depressed melting temperature, n=2 for cylindrical pores and n=3 for spherical pores.

$$R_p = -\frac{32.33}{\triangle T} + 0.68 \tag{5}$$

$$R_p = -\frac{64.67}{\triangle T} + 0.57 \tag{6}$$

$$V_{pore} = V_{ice}(\frac{r+\delta}{r})^n \tag{7}$$

The accumulated pore volume and the pore size distribution calculated for the studied concrete samples are shown in Figure 6, Figure 7 and Figure 8. Taking the concrete mixes with w/c=0.5 as an example (Figure 7), it is observed that the accumulated pore size distribution curve as calculated for the capillary saturated sample is below the curve for the vacuum saturated sample from 50 nm up to about 5 nm for both C504 and C506. That is to say in terms of the detected pores, a larger proportion of pores with relatively smaller pore radii is found in the capillary saturated samples than that in the vacuum saturated samples. For sample C504 (Figure 7b), the calculated volume for the pores with radii between about 2 nm to about 9 nm in the capillary saturated sample is bigger than that in its vacuum saturated counterpart based on the cylindrical assumption; while for the spherical assumption, there are more pores with the radii between about 2 nm to about 11 nm. The similar trend can also be found for sample C506 (Figure 7d).

Actually, the porosity of the same concrete mix should be independent of the saturation methods. With respect to the difference of the calculated pores as observed, a possible explanation could be as follows. As discussed in Section 2, the melting temperature depression ΔT for the ice confined in the non-fully-saturated pores is larger than that in the fully saturated pores. Since the relation of ΔT and R_p adopted in the calculation is based on the full saturation assumption, the pore radii derived for the non-fully saturated pores are actually underestimated. In other words, we will detect more small pores for a sample if the pores under study are not fully saturated compared with the fully saturated sample.As indicated in Figure 7, a high proportion of small pores are found for the capillary saturated samples compared with the vacuum saturated samples. That is to say possibly

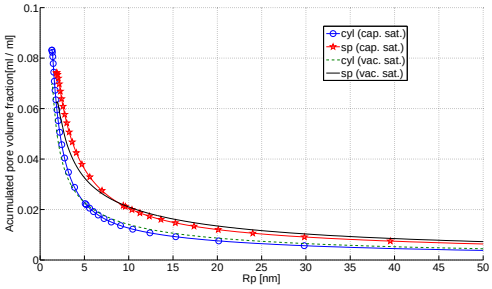

(a) Accumulated pore volume fraction for sample C404.

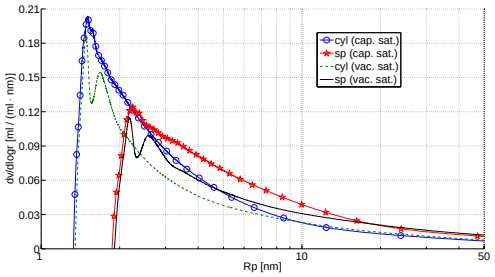

(b) Pore size distribution for sample C404.

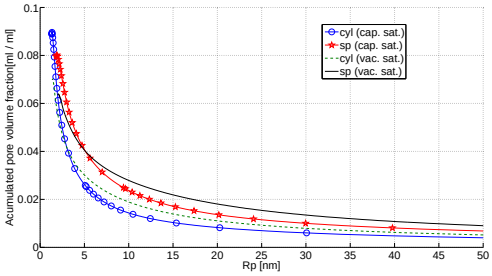

(c) Accumulated pore volume fraction for sample C406.

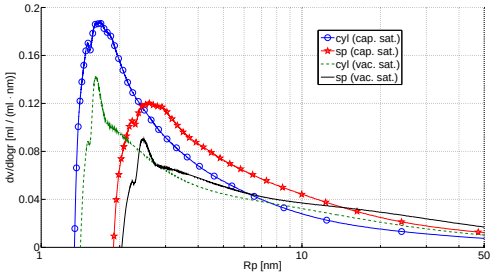

(d) Pore size distribution for sample C406.

Figure 6: Accumulated volume fraction of the pores with radii smaller than 1 μm (assumption made) by the total volume of the sample and the pore size distribution for the concrete mixes with w/c=0.40. The pore shape is assumed to be cylindrical (cyl) and spherical (sp) in the comparison.

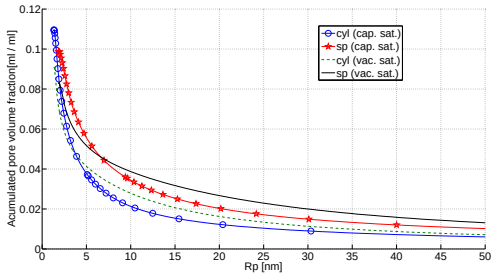

(a) Accumulated pore volume fraction for sample C504.

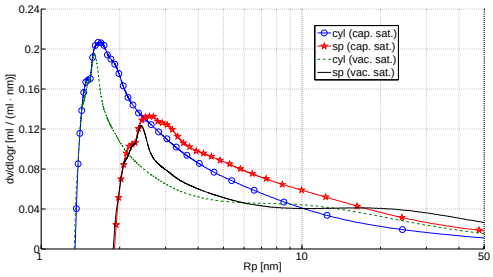

(b) Pore size distribution for sample C504.

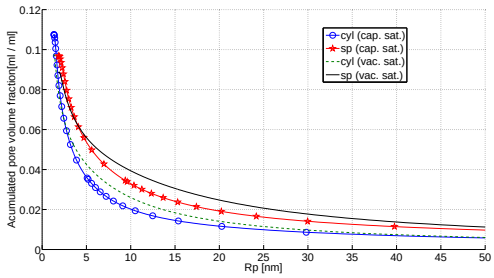

(c) Accumulated pore volume fraction for sample C506.

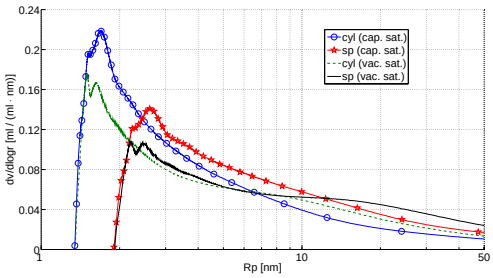

(d) Pore size distribution for sample C506.

Figure 7: Accumulated volume fraction of the pores with radii smaller than 1 μm (assumption made) by the total volume of the sample and the pore size distribution for the concrete mixes with w/c=0.50. The pore shape is assumed to be cylindrical (cyl) and spherical (sp) in the comparison.

the pores with the radii as shown in Figure 7 for the capillary saturated samples may not be fully saturated. Then, one may argue that this is not relevant since we can find a portion of water present in the big air entrained pores. If the big air entrained pores have already been filled with some amount of water, the pores with radii much smaller than that of the air entrained voids should have been saturated considering the magnitude of the capillary suction pressure. A possible explanation for the non-fully saturation of the very mall pores in the capillary saturated samples could be due to the cryogenic suction or cryosuction in the freezing process, which is the effect of water from neighboring pores or from the surroundings being drawn towards ice crystals already created in the pore system [29, 61–64]. Since the entrained air voids are only partly filled in the capillary saturated samples and the water in these pores will freeze at higher temperatures than that in the small nm scale pores, part of the water in the small nm scale pores could possibly be drawn to the big pores, leaving the small pores in non-fully saturated condition during the freezing/melting process. While there is little or no room for this water movement for the fully saturated samples, the small pores under study will stay fully saturated.

A simplified schematic illustration about the comparison between the same pore systems under the non-fully and the fully saturated conditions during freezing are shown in Figure 9. It should be noted that the menisci system in the drawing (corresponding to Case A in Figure 1) is just an example and the conclusion will not be changed if the menisci system is different from the drawing. At the beginning, pore A and B can be fully saturated (due to capillary force) but pore C could be

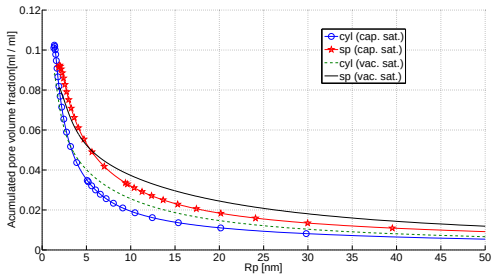

(a) Accumulated pore volume fraction for sample C602.

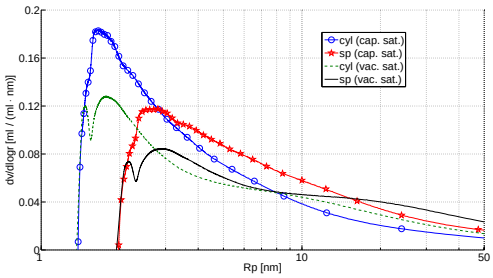

(b) Pore size distribution for sample C602.

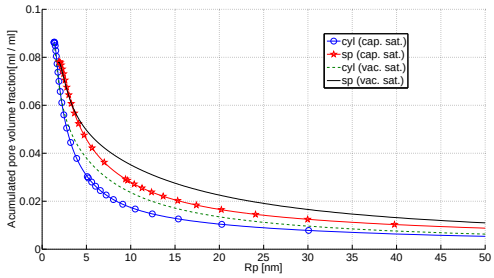

(c) Accumulated pore volume fraction for sample C606.

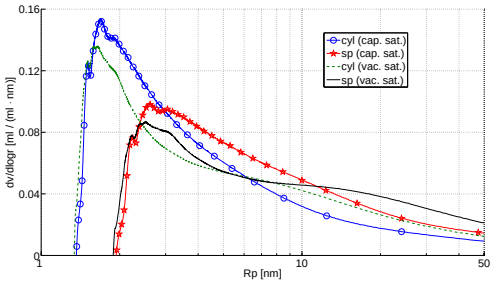

(d) Pore size distribution for sample C606.

Figure 8: Accumulated volume fraction of the pores with radii smaller than 1 μm (assumption made) by the total volume of the sample and the pore size distribution for the concrete mixes with w/c=0.60. The pore shape is assumed to be cylindrical (cyl) and spherical (sp) in the comparison.

non-fully saturated under the non-fully saturated condition (left); while under the fully saturated condition (right), all of these three pores are saturated. As the temperature decreases to the point that the liquid in pore C under fully saturated condition can freeze, the water in pore C under the non-fully saturated condition will stay unfrozen due to the gas phase inside of the pore, which leads to the further depression of the freezing point of the inside water. When the temperature keeps decreasing, the liquid in pore C under the non-fully saturation (left) will freeze at a certain temperature. Meanwhile, due to the cryosuction effect, part of the water in pore A and B which are connected to the non-fully saturated pore C could be sucked out. It is noted that the water migration caused by the cryosuction could possibly take place over the whole freezing process, as far as there is still empty space. Consequently, pore A and B will be under non-fully saturated situation when the confined water freezes. Then the measured freezing/melting point of the water in the non-fully saturated pore A and B (even though they are fully saturated at the beginning) will be lower compared with their fully saturated counterparts, as illustrated in Figure 9. The lower the freezing/melting point, the smaller the calculated pore size. Since the relation between the pore size and the measured freezing/melting point in the adopted calculation is based on the fully saturated condition, the calculated radii of the non-fully saturated pores will be smaller compared with that under fully saturation. Thus, it should be kept in mind that the high proportion of the small pores as calculated for the capillary saturated samples may not be relevant. In the context of pore size analysis using freezing/melting point depression, due to fact that it is almost impossible to derive the quantitative relation between the depressed freezing/melting point and the corresponding pore sizes as discussed in Section 2, it is not appropriate to calculate the pore size distribution for the samples whose pores under study are not fully saturated.

It is also noticed that the total accumulated pore volume as calculated (less than 1 μm by the assumption made before) for the capillary saturated samples is larger than that of the vacuum saturated samples, see Figure 7a and Figure 7c. As demonstrated before, the relation of the pore volume and the ice volume is given as Eq.7. By taking into account the volume of the $\delta-$layer, which could account for an important part of the total pore volume when the pore radii are very small, the pore volume as derived for the capillary saturated samples could be larger than that of the vacuum saturated samples, even if the saturation degree of the small pores in the capillary saturated samples during freezing/melting could be lower than that in the vacuum saturated samples. The reason is that the calculated pore sizes of the capillary saturated samples are smaller than that in the vacuum saturated samples (smaller pore sizes indicates more surface area), then the estimated volume of the $\delta-$layer for the capillary saturated samples could be higher than that of the vacuum saturated samples (the related volume comparison can be found in Table 2), leading to the bigger total accumulated volume as observed in the capillary saturated samples.

Similar phenomena which we have observed for the concrete mixes with w/c=0.5 have also been found for the concrete mixes with w/c=0.4 (Figure 6) and w/c=0.6 (Figure 8). The proposed explanations with respect to the obtained results given for the concrete mixes with w/c=0.5 are applicable to all of the concrete mixes studied.

Although it is not possible to determine the pore size distribution for the pores with radii bigger than the upper limit of the LTC method, the volume of the proportion of big pores in the concrete samples can be estimated from Figure 3. In the previous discussion, the accumulated pore volume for the pores with radii smaller than 1 μm were calculated by making certain assumptions. For the bigger pores (radii >1 μm) in this study, the pore volume is assumed to be the same as that of the ice without considering the volume of $\delta-$layer which is thought to be not an important part compared with the total pore volume of these big pores. By adding the volume of the big pores, i.e.,

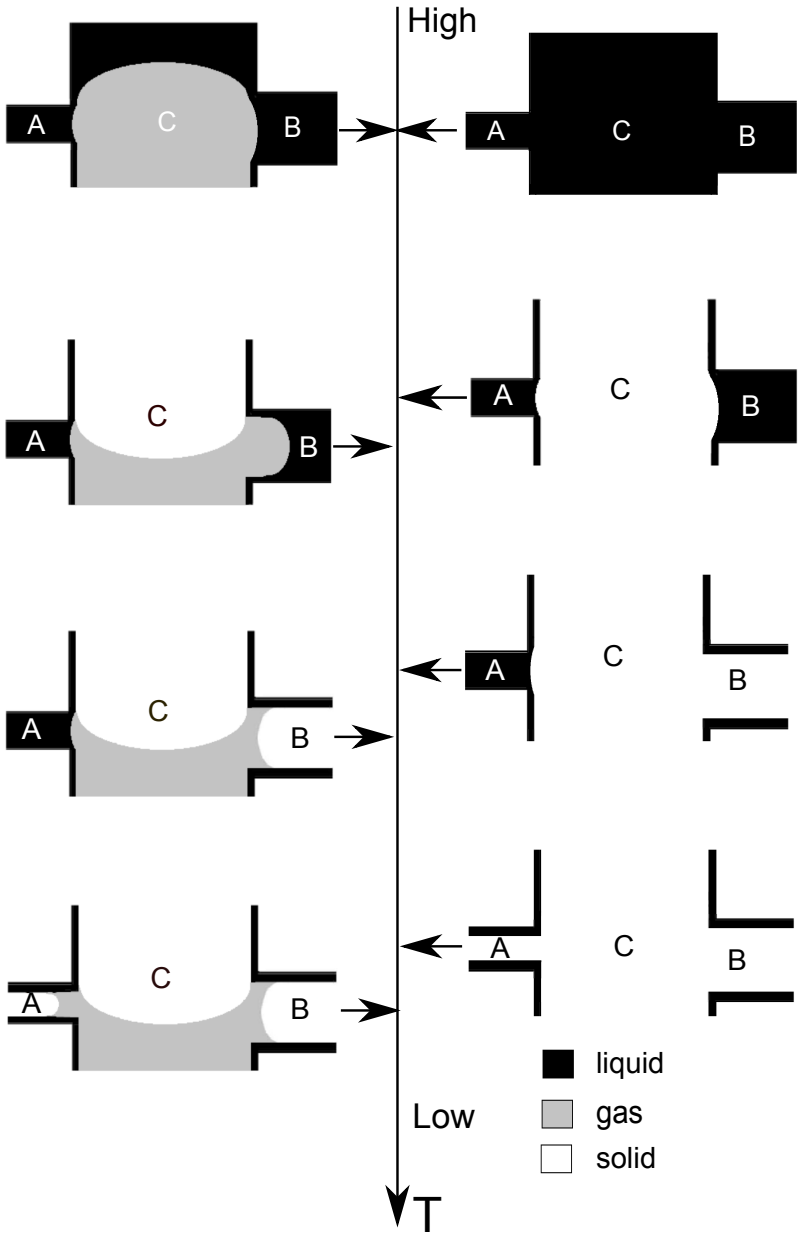

Figure 9: A simplified schematic illustration of the comparison between the same pore systems under the non-fully saturated (left) and the fully saturated (right) conditions during freezing, pore shape being assumed to be cylindrical and the pore radius $r_C > r_B > r_A$. The three pores are not isolated and they are connected to other pores. The dark area close to the pore wall indicates liquid in the $\delta-$layer. The temperature decreases along the line (T) from the top to the bottom. Details about the change of the liquid-gas and solid-gas curvature in the pores to meet the thermodynamic conditions as the temperature decreases are neglected in the drawing. Compared with pores under fully saturation, the calculated radii of the pores with the same radii under non-fully saturation will be smaller due to higher temperature depressions.

Table 2: The calculated pore volume fraction detected by LTC, the volume fraction of the estimated $\delta-$layer and the volume fraction of the pores with radii less than 0.8 nm for the concrete samples presented in Figure 3 based on cylindrical (cyl.) and spherical (sp.) pore shape assumption. The volume fraction is the volume by the total volume of the sample. The notation for the sample C404c means that w/c=0.40, nominal air content 4%, capillary saturated, and likewise ("v" indicating vacuum saturated) for the other samples. The specific surface area is also listed.

Sample	Pore vol. fraction (%)[a,b]		$\delta-$layer vol. fraction (%)[b]		Pore vol. fraction (%)[c,d] ($R_p < 0.8$ nm)		Total specific surface area (m^2/g)[e]	
	cyl.	sp.	cyl.	sp.	cyl.	sp.	cyl.	sp.
C404c	10.4	9.6	4.0	3.2	5.8	6.7	30.3	24.4
C404v	11.6	11.0	3.2	2.5	6.0	6.7	24.0	19.3
C406c	11.9	11.0	4.3	3.3	5.0	5.9	31.5	25.2
C406v	13.2	12.5	2.5	1.9	7.6	8.3	25.9	20.8
C504c	13.5	12.5	4.7	3.7	4.4	5.4	35.5	28.4
C504v	13.7	12.8	3.7	2.9	5.6	6.4	26.6	21.4
C506c	13.6	12.5	4.8	3.7	3.6	4.7	35.4	28.3
C506v	16.0	15.1	3.9	3.0	5.6	6.6	28.4	22.7
C602c	13.5	12.5	4.6	3.6	3.4	4.5	32.4	25.8
C602v	13.5	12.7	3.4	2.7	4.5	5.3	24.6	19.6
C606c	12.3	11.4	3.5	2.7	4.0	4.8	26.7	21.2
C606v	18.1	17.4	3.2	2.4	4.2	4.9	24.3	19.4

Note: a). the pore volume fraction detected by the LTC method; b). the volume of the the $\delta-$layer in the pores with radii bigger than 1 μm (assumption made) is not included; c). this fraction is estimated by using the measured total water content in the tested sample; d). it should be noted that this value might be overestimated due to the procedure adopted to measure the total water content, i.e., drying at 105 °C till constant weight; e). the total surface area is expressed in m^2 per gram dry concrete and the total specific surface area calculated does not include the contribution from the pores with radii smaller than the thickness of the $\delta-$layer and that from the pores with radii bigger than 1 μm (assumption made).

the ice volume of these pores, the total accumulated pore volume detected by LTC method can be estimated. The volume of the $\delta-$layer (in pores with radii smaller than 1 μm) can be calculated by subtracting the calculated total ice content from the calculated total pore volume. Meanwhile, it is realized that the volume of the pores with radii smaller than the thickness of the $\delta-$layer (0.8 nm) cannot be detected by the LTC method directly because this part of water will also stay unfrozen during the testing. However, it is still possible to estimate the volume. As mentioned in Section 3, the total water content of a sample can be obtained through the gravimetric measurements. Thus the volume of the unfreezable water in the pores with radii smaller than the thickness of the $\delta-$layer can be estimated by subtracting the volume of the total ice and the volume of the $\delta-$layer from the volume of the total water. Furthermore, it is also possible to estimate the specific surface area from the pore volume based on the assumed pore shape. For the pores with a radii of R_p and the volume of V_{pore}, the corresponding specific surface area (S) can be calculated by Eq.8, where n=2 for cylindrical pores and n=3 for spherical pores. By summing up all the specific surface area

of the pores detected, the total specific surface area can be obtained. However, the total specific surface area calculated in this study does not include the contribution from the surfaces of pores with radii smaller than the thickness of the $\delta-$layer and that from the pores with radii bigger than 1 μm. Thus, it is no more than a rough estimation. The calculated results are listed in Table 2.

$$S = \frac{n \cdot V_{pore}}{R_p} \tag{8}$$

According to Table 2, it can be seen that for the same concrete mix, the total pore volume fraction determined is normally larger in the vacuum saturated sample compared with that in the capillary saturated sample, because the saturation degree in the capillary saturated sample is lower. The calculated volume of the $\delta-$layer is found to be larger in the capillary saturated samples compared with the vacuum saturated counterparts. The reason is that due to the further depressed phase transition point of water/ice in the capillary saturated samples, the pore radii of the capillary saturated samples are wrongly interpreted and smaller values than that in the vacuum saturated samples are obtained. For a certain pore volume, it can be imagined that the surface area of pores with smaller pore radii should be larger than that of the pores with bigger pore radii. Since the volume of the $\delta-$layer is calculated by multiplying the calculated surface area and the thickness of the $\delta-$layer, which is assumed to be a constant value (0.8 nm assumed in this study), larger surface area results into larger apparent volume in the $\delta-$layer. When the pore radii are on the order of several nm, the volume of the $\delta-$layer could be an important part of the total pore volume. As mentioned before, after adding the volume of $\delta-$layer, the total pore volume (radii<1 μm) for the capillary saturated samples could be larger than that of the vacuum saturated ones even if the saturation degree of the pores during freezing/melting is lower in the capillary saturated samples.

As expected, the calculated total specific surface area does show that the value of the vacuum saturated samples is smaller than that of the capillary saturated samples. The reason has just been explained, i.e., the further depressed phase transition point of water/ice in the capillary saturated samples. It needs to be mentioned that the specific surface area present here is expressed in m^2 per gram dry concrete. The reported value for the relevant fully hydrated cement pastes in literature is between 80 to 300 m^2 per gram of dry paste depending on several different measuring techniques used, e.g., see [8, 9, 12]. A rough conversion of the unit shows that the the specific surface area of the studied concrete samples is around 100 m^2 per gram of dry paste, which falls nicely in the reported range. Therefore, it seems that the surface area calculation might not be affected by the pores with radii smaller than the thickness of the $\delta-$layer. This is somewhat in accordance with the argument given by Thomas et al. [9], which states the interlayer spaces (sizes comparable to the thickness of the $\delta-$layer) within the C-S-H phase do not contribute to surface area as it is normally defined. That is, possibly the LTC method can be used in the context of surface area determination irrespective of the fact that it cannot detect the pores with radii smaller than the thickness of the $\delta-$layer. Additionally, it should also be noted that the calculated volume of the $\delta-$layer and the total specific surface area for the capillary saturated samples are only apparent values, which do not necessarily represent the true values due to the effect of the further depressed phase transition point of the water/ice confined in the non-fully saturated pores.

4.3. Comparison of the hysteresis

Regarding the more pronounced hysteresis effect observed in the capillary saturated samples than the vacuum saturated samples, e.g., in the temperature range of -10 °C to -40 °C, possible explanations could be proposed. Using the sample C606 as an example, the calibrated ice volume

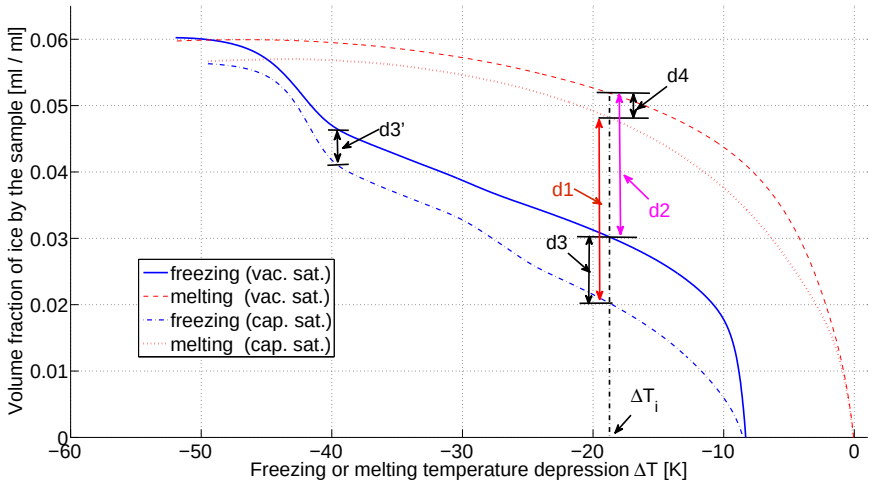

Figure 10: The ice volume fraction of the pores with radii smaller than 1μm (assumption made) versus the calibrated freezing/melting temperature depression for sample C606 to illustrate the more pronounced hysteresis effect found for the capillary saturated sample than the vacuum saturated sample.

fraction diagram for the pore size distribution analysis in the study (i.e., the ice in the pores which are smaller than 1 μm by the assumption, meaning the ice in big air voids is not included) is shown in Figure 10. It can be found that the total ice volume for the capillary saturated sample is smaller than that of the vacuum saturated one, which could be due to the lower saturation degree of the capillary saturated sample during the freezing/melting process. Under the same temperature depression ΔT_i, the distance between the freezing curve and the melting curve of the capillary saturated sample is denoted as $d1$ and that of the vacuum saturated sample is denoted as $d2$, while $d3$ denotes the distance between the two freezing curves and $d4$ for the melting curves. The lower saturation degree of the capillary saturated sample is believed to partly contribute to $d3$ and $d4$. Another contribution factor could be attributed to the fact that the freezing/melting temperature for the water/ice confined in pores with certain radius will be further depressed for the non-fully-saturated sample. Thus, a portion of water /ice which should freeze/melt at certain temperature if the pores are fully saturated will freeze/melt at a lower temperature since the pores are not fully saturated. This will result in that the freezing/melting curve of the non-fully-saturated sample will be lower than fully saturated one during certain pore radii. One may argue that the further depressed freezing/melting temperature behavior for the non-fully saturated sample should take place both in the freezing and melting process, so the the contribution due to this further depression to $d3$ and $d4$ should be the same. If so, why is the hysteresis still more pronounced in the non-fully saturated sample?

According to the explanation given by Brun et al. [24], pore shape is kind of the main reason for the hysteresis. In another word, there will be hysteresis if the pore shape is cylindrical and there will not be any hysteresis at all if the pores are spherical. Since the pores are neither perfectly cylindrical nor spherical in reality, they developed a shape factor to characterize a specific pore system. Based on their arguments, it would be more appropriate to adopt the cylindrical assumption for the studied concrete samples since the hysteresis is very pronounced. As a result of this hypothesis, the

pore radii corresponding to the same temperature depression ΔT in the freezing and the melting should be different. Taking the ΔT = -10°C for example, the corresponding pore radius is about 6-7 nm (Eq.6) in freezing and is about 3 nm (Eq.5) in melting. Analogously, the distance $d4$ between the melting curves in the current position on the Figure 10 should not correspond to $d3$ between the freezing curves at the same ΔT, but a position with a lower temperature whose corresponding radius is the same as that in the melting, e.g., $d3'$. On the other hand, as can be found in Figure 8d based on the cylindrical pore assumption, the volume of the pores predicted by the capillary saturated sample is bigger than that of the vacuum saturated sample for the pores whose radii are smaller than about 6 nm till about 2 nm. This is, the water confined in these pores in the capillary saturated sample is further depressed due to the non-fully saturated condition, with the corresponding freezing point mainly between -10 °C to -40 °C. So for the melting curve at ΔT = -10 °C, the effect due to the non-fully saturated pores on the total ice volume is almost completely reflected while this effect is just starting to show on the freezing curve. As a result, $d3$ is always bigger than $d4$ at the same temperature depression during the temperature range of -10 °C to -40 °C. The consequence is that $d1$ is always bigger than $d2$ for a certain ΔT during the temperature range, showing more pronounced hysteresis effect in the capillary saturated samples compared with the vacuum saturated samples. Due to the supercooling in the freezing curves, the hysteresis is not analyzed for the temperature depression less than -10 °C. When the temperature depression goes down to lower than -40 °C, the hysteresis effect tends to be the same magnitude for capillary and vacuum saturated samples and finally the hysteresis will disappear. However, it is also noted that the pore shape may not be the only reason for the hysteresis. More discussion about the origin of the hysteresis behavior, which can be found in, e.g., [7, 65–67], falls outside the scope of this discussion.

5. Conclusions

Low temperature (micro-)calorimetry (LTC) is often adopted to study the pore volume and the pore size distribution of porous materials. It is noted that if the porous material under testing is not fully saturated, not only the pore volume is underestimated but also the relevance of the derived pore size distribution would be in doubt. The present study carefully examined theoretically the thermodynamic relation between the pore size and the depressed freezing/melting temperature of the confined water/ice under fully and non-fully saturated conditions and the impact of sample saturation on the analysis of the pore volume and the pore size distribution was illustrated using experimental data measured on hardened concrete samples. Some key points can be summarized as follows:

1. The thermodynamic background about the freezing/melting point of water/ice confined in a pore under fully and non-fully saturated conditions were carefully examined. It is emphasized that compared with the situation when the pore is fully saturated, the freezing/melting point of the pore water/ice is lower if the pore is not fully saturated.
2. The ice content calculated from the capillary saturated sample was lower than that from the vacuum saturated sample for the same concrete mix and the difference became bigger as the nominal air content increases. This implies that the capillary saturation may not be able to saturate all the pores, especially the entrained air voids, in the concrete samples. Then, part of the water in some of the initially saturated very small pores (at the nanometric level) before freezing starts may be sucked out by the cryo-suction force during the freezing process, leaving some of the very small pores also under non-fully saturated condition.

3. The proportion of the calculated pores with smaller radii was higher in the capillary saturated samples than that in the vacuum saturated samples using the same calculation method. The reason is probably that for the capillary saturated samples, not all of the pores under study are fully saturated during the freezing/melting process and thus the corresponding phase transition temperatures for the water/ice confined in these pores are further depressed, as illustrated in the theoretical study. Then, the pore radii would be wrongly interpreted as we still abide by the relation as derived based on the full saturation. However, since the relation for the non-fully saturated pores is extremely difficult, if it is still possible, to define, it is not appropriate to derive the pore size distribution in the context of LTC analysis using non-fully saturated samples.
4. The hysteresis behavior observed between the freezing and melting ice content curves in the capillary saturated samples was more pronounced compared with that in the vacuum saturated samples. Possibly it could also be related to the further depressed phase transition temperatures for the water/ice in the non-fully saturated pores as described in a detailed manner in the discussion.

Acknowledgment

The research leading to these results has received funding from the European Union Seventh Framework Programme (FP7/2007-2013) under grant agreement 264448.

References

[1] T. Powers, The air requirement of frost resistant concrete, in: Proceedings of the Highway Research Board, Vol. 29, 1949, pp. 184–211.

[2] M. Pigeon, R. Pleau, Durability of concrete in cold climates, no. 4, Taylor & Francis, 1995.

[3] S. Kosmatka, W. Panarese, Design and control of concrete mixtures, Portland Cement Association, 2002.

[4] T. Powers, T. Brownyard, Studies of the physical properties of hardened portland cement paste, in: ACI Journal Proceedings, Vol. 43, 1947, pp. 549–602.

[5] H. Jennings, Refinements to colloid model of C–S–H in cement: CM–II, Cement and Concrete Research 38 (3) (2008) 275–289.

[6] P. McDonald, V. Rodin, A. Valori, Characterisation of intra-and inter-C–S–H gel pore water in white cement based on an analysis of NMR signal amplitudes as a function of water content, Cement and Concrete Research 40 (12) (2010) 1656–1663.

[7] Z. Sun, G. Scherer, Pore size and shape in mortar by thermoporometry, Cement and Concrete Research 40 (5) (2010) 740–751.

[8] R.F.Feldman, The porosity and pore structure of hydrated portland cement paste, in: J. S. L.R. Roberts (Ed.), Pore Structure and Permeability of Cement based Materials, Vol. 137, Materials Research Society, Pittsburgh, PA, 1989, pp. 59–73.

[9] J. Thomas, H. Jennings, A. Allen, The surface area of hardened cement paste as measured by various techniques, Concr. Sci. Eng 1 (1999) 45–64.

[10] A. Kjeldsen, M. Geiker, On the interpretation of low temperature calorimetry data, Materials and Structures 41 (1) (2008) 213–224.

[11] J. Strange, J. Mitchell, J. Webber, Pore surface exploration by NMR, Magnetic Resonance Imaging 21 (3-4) (2003) 221–226.

[12] V. Baroghel-Bouny, Water vapour sorption experiments on hardened cementitious materials: Part I: Essential tool for analysis of hygral behaviour and its relation to pore structure, Cement and Concrete Research 37 (3) (2007) 414–437.

[13] J. Villadsen, Pore structure in cement based materials, Tech. Rep. 277, Building Materials Laboratory, Technical University, Denmark (1992).

[14] J. Young, A review of the mechanisms of set-retardation in portland cement pastes containing organic admixtures, Cement and Concrete Research 2 (4) (1972) 415–433.

[15] G. Fagerlund, Determination of pore-size distribution from freezing-point depression, Materials and Structures 6 (3) (1973) 215–225.

[16] Q. Xu, J. Hu, J. Ruiz, Z. Wang, K.and Ge, Isothermal calorimetry tests and modeling of cement hydration parameters, Thermochimica Acta 499 (1) (2010) 91–99.

[17] B. Johannesson, Dimensional and ice content changes of hardened concrete at different freezing and thawing temperatures, Cement and Concrete Composites 32 (1) (2010) 73–83.

[18] Q. Xu, J. M. Ruiz, J. Hu, K. Wang, R. Rasmussen, Modeling hydration properties and temperature developments of early-age concrete pavement using calorimetry tests, Thermochimica Acta 512 (1) (2011) 76–85.

[19] D. Bager, Ice formation in hardened cement paste, Ph.D. thesis, Building Materials Laboratory, Technical University of Denmark (1984).

[20] D. Bager, E. Sellevold, Ice formation in hardened cement paste, Part I–room temperature cured pastes with variable moisture contents, Cement and Concrete Research 16 (5) (1986) 709–720.

[21] D. Bager, E. Sellevold, Ice formation in hardened cement paste, Part III-slow resaturation of room temperature cured pastes, Cement and Concrete Research 17 (1) (1987) 1–11.

[22] E. Sellevold, D. Bager, Some implications of calorimetric ice formation results for frost reistance testing of concrete, in Beton og Frost, Dansk Betonforening 22 (1985) 47–74.

[23] R. Defay, I. Prigogine, A. Bellemans, D. Everett, Surface tension and adsorption, Longmans London, 1966.

[24] M. Brun, A. Lallemand, J. Quinson, C. Eyraud, A new method for the simultaneous determination of the size and shape of pores: the thermoporometry, Thermochimica Acta 21 (1) (1977) 59–88.

[25] G. Fagerlund, Studies of the scaling, the water uptake and the dilation of specimens exposed to freezing and thawing in NaCl solution, in: Proceedings of RILEM committee 117 DC Freezing/thaw and de-icing resistance of concrete, Swden, 1991, pp. 37–66.

[26] M. Brun, A. Lallemand, J. Quinson, C. Eyraud, Changement d'état liquid–solide dans les milieux poreux. II. Étude théorique de la solidification d'un condensate capillaire (liquid–solid change of state in porous media. II. Theoretical study of the solidification of a capillary condensate), J.Chim.Phys. 6 (1973) 979–989.

[27] T. Powers, Physical properties of cement paste, in: Proc. Fourth Int. Symp. on the Chemistry of Cement, Washington, DC, 1960.

[28] J. Schmelzer (Ed.), Nucleation Theory and Applications, WILEY-VCH, 2005.

[29] G. Scherer, Freezing gels, Journal of non-crystalline solids 155 (1) (1993) 1–25.

[30] J. Kaufmann, Experimental identification of ice formation in small concrete pores, Cement and Concrete Research 34 (8) (2004) 1421–1427.

[31] J. Quinson, M. Astier, M. Brun, Determination of surface areas by thermoporometry, Applied Catalysis 30 (1) (1987) 123–130.

[32] J. Quinson, M. Brun, Progress in thermoporometry, K. K. Unger, J. Rouquerol, K. S.W Sing and H. Kral (eds): Characterization of Porous Solids, Elsevier, Amsterdam (1988) 307.

[33] D. Rasmussen, A. MacKenzie, Clustering in supercooled water, The Journal of Chemical Physics 59 (1973) 5003–5013.

[34] H. Jellinek (Ed.), Water Structure at the Water-Polymer Interface, Plenum, New York, 1972.

[35] K. Ishikiriyama, M. Todoki, K. H. Min, S. Yonemori, M. Noshiro, Pore size distribution measurements for microporous glass using differential scanning calorimetry, Journal of Thermal Analysis and Calorimetry 46 (3-4) (1996) 1177–1189.

[36] M. Landry, Thermoporometry by differential scanning calorimetry: experimental considerations and applications, Thermochimica acta 433 (1-2) (2005) 27–50.

[37] C. Le Sage de Fontenay, Ice formation in hardened cement paste (in Danish), Ph.D. thesis, Building Materials Laboratory, Technical University of Denmark (1982).

[38] K. Fridh, Internal frost damage in concrete–experimental studies of destruction mechanisms, Ph.D. thesis, Division of Building Materials, Lund Institute of Technology (2005).

[39] E. Hansen, H. Gran, E. Sellevold, Heat of fusion and surface tension of solids confined in porous materials derived from a combined use of NMR and calorimetry, The Journal of Physical Chemistry B 101 (35) (1997) 7027–7032.

[40] F. Radjy, E. Sellevold, K. Hansen, Isosteric vapor pressure-temperature data for water sorption in hardened cement paste: enthalpy, entropy and sorption isoterms at different temperatures, Tech. Rep. 57, Department of Civil Engineering, Technical University of Denmark (2003).

[41] M. Wu, B. Johannesson, M. Geiker, Determination of ice content in hardened concrete by low temperature calorimetry: influence of baseline calculation and heat of fusion of confined water, Journal of Thermal Analysis and Calorimetry 115 (2) (2014) 1335–1351.

[42] T. Yamamoto, A. Endo, Y. Inagi, T. Ohmori, M. Nakaiwa, Evaluation of thermoporometry for characterization of mesoporous materials, Journal of Colloid and Interface Science 284 (2) (2005) 614–620.

[43] J. Banys, M. Kinka, J. Macutkevic, G. Völkel, W. Böhlmann, V. Umamaheswari, M. Hartmann, A. Pöppl, Broadband dielectric spectroscopy of water confined in MCM–41 molecular sieve materials–low-temperature freezing phenomena, Journal of Physics: Condensed Matter 17 (2005) 2843.

[44] K. Ishikiriyama, M. Todoki, K. Motomura, Pore size distribution (PSD) measurements of silica gels by means of differential scanning calorimetry I. optimization for determination of PSD, Journal of colloid and interface science 171 (1) (1995) 92–102.

[45] M. Setzer, Mechanical stability criterion, triple-phase condition, and pressure differences of matter condensed in a porous matrix, Journal of Colloid and Interface Science 235 (1) (2001) 170–182.

[46] M. Setzer, Micro-ice-lens formation in porous solid, Journal of Colloid and Interface Science 243 (1) (2001) 193–201.

[47] G. Scherer, J. Valenza II, Materials Science of Concrete, Vol. VII, 2005, Ch. Mechanisms of Frost Damage, pp. 209–246.

[48] P. Williams, Properties and behavior of freezing soils, Tech. Rep. 72, Norwegian Geotechnical Institute, Oslo,Norway (1961).

[49] J. Blachere, J. Young, The freezing point of water in porous glass, Journal of the American Ceramic Society 55 (6) (1972) 306–308.

[50] E. Shiko, K. Edler, J. Lowe, S. Rigby, Probing the impact of advanced melting and advanced adsorption phenomena on the accuracy of pore size distributions from cryoporometry and adsorption using NMR relaxometry and diffusometry, Journal of Colloid and Interface Science 385 (1) (2012) 183–192.

[51] B. Johannesson, Moisture fixation in mature concrete and other porous materials (8A), lecture notes for Introduction to Concrete Technology (11563), Technical University of Denmark (2011).

[52] B. Johannesson, G. Fagerlund, Concrete for the storage of liquid petroleum gas–freeze/thaw phenomena and durability at freezing to -50 °C, Report TVBM– 7174, Division of Building Materials, Lund Institute of Technology (2003).

[53] G. Fagerlund, B. Johannesson, Concrete for the storage of liquid petroleum gas, part ii: influence of very high moisture contents and extremely low temperatures, -196 °C, Report TVBM - 1851, Division of Building Materials, Lund Institute of Technology (2005).

[54] RILEM recommendations–absorption of water by immersion under vacuum, Materials and Structures 101 (1984) 393–394.

[55] M. Geiker, P. Laugesen, On the effect of laboratory conditioning and freeze/thaw exposure on moisture profiles in HPC, Cement and Concrete Research 31 (12) (2001) 1831–1836.

[56] A. Henrichsen, P. Laugesen, M. Geiker, E. J. Pedersen, N. Thaulow, HETEK: method for test of the frost resistance of high performance concrete : summary, conclusions and recommendations, Tech. Rep. 97, The Danish Road Directirate, Denmark Minstry of Transport (1997).

[57] M. I. Khan, A novel method for measuring porosity of high strength concrete, in: Proceedings of the 7th Saudi Engineering Conference (SEC7), Dec, 2007.

[58] K. Ishikiriyama, M. Todoki, Pore size distribution measurements of silica gels by means of differential scanning calorimetry II. thermoporosimetry, Journal of Colloid and Interface Science 171 (1) (1995) 103–111.

[59] K. Ishikiriyama, M. Todoki, Evaluation of water in silica pores using differential scanning calorimetry, Thermochimica Acta 256 (2) (1995) 213–226.

[60] M. Titulaer, J. Van Miltenburg, J. Jansen, J. Geus, Thermoporometry applied to hydrothermally aged silica hydrogels, Recueil des Travaux Chimiques des Pays-Bas 114 (8) (1995) 361–370.

[61] O. Coussy, T. Fen-Chong, Crystallization, pore relaxation and micro-cryosuction in cohesive porous materials, Comptes Rendus Mecanique 333 (6) (2005) 507–512.

[62] P. Monteiro, O. Coussy, D. Silva, Effect of cryo-suction and air void transition layer on hydraulic pressure of freezing concrete, ACI Materials Journal 103 (2) (2006) 136–140.

[63] A. Dupas, Effect of vertical drain barrier on road behaviour in freeze-thaw periods, in: Geotextiles, Geomembranes and Related Products, Volume 1 (out of 3 volumes): Proceedings of the 4th International Congress, The Hague, 28 May-1 June 1990, Vol. 1, Taylor & Francis, 1990, p. 339.

[64] P. Parker, A. Collins, Dehydration of flocs by freezing, Environmental Science & Technology 33 (3) (1999) 482–488.

[65] K. Morishige, K. Kawano, Freezing and melting of water in a single cylindrical pore: The pore-size dependence of freezing and melting behavior, The Journal of Chemical Physics 110 (1999) 4867.

[66] G. Findenegg, S. Jähnert, D. Akcakayiran, A. Schreiber, Freezing and melting of water confined in silica nanopores, ChemPhysChem 9 (18) (2008) 2651–2659.

[67] J. Riikonen, J. Salonen, V. Lehto, Utilising thermoporometry to obtain new insights into nanostructured materials (review part 1), Journal of Thermal Analysis and Calorimetry 105 (2011) 811–821.